Numerical Integration of the Shallow-Water Equations on a Twisted Icosahedral Grid. Part II: A Detailed Description of the Grid and an Analysis of Numerical Accuracy

ROSS HEIKES AND DAVID A. RANDALL

Department of Atmospheric Science, Colorado State University, Fort Collins, Colorado

(Manuscript received 23 February 1994, in final form 14 November 1994)

ABSTRACT

The finite-difference scheme for the Laplace and flux-divergence operators described in the companion paper (Part I) is consistent when applied on a grid consisting of perfect hexagons. The authors describe a necessary and sufficient condition for this finite-difference scheme to be consistent when applied on a grid consisting of imperfect hexagons and pentagons, and present an algorithm for generating a spherical geodesic grid on a sphere that guarantees that this condition is satisfied. Also, the authors qualitatively describe the error associated with the operators and estimate their order of accuracy when applied on the new grid.

1. Introduction

A companion paper, Heikes and Randall (1995; hereafter referred to as Part I) discussed the design of a finite-difference shallow-water model constructed on a spherical geodesic grid and presented some numerical results. The present paper describes in detail the grid used in the model. In particular, we show that the simple algorithm outlined in section 3 of Part I leads to a grid for which the spatial differencing operators are inconsistent, that is, for which the truncation errors associated with the finite-difference operators do not go to zero as the cell size decreases to zero. A modified algorithm presented in this paper allows consistency and improved numerical accuracy.

2. Some observations about the Laplace operator and the simple spherical geodesic grid

Following the development in section 4 of Part I, by Gauss' theorem we have

$$\int_A \nabla^2 \alpha dA = \oint_C \frac{\partial \alpha}{\partial n} dC, \tag{1}$$

where α is an arbitrary scalar function, A is some arbitrary region in the plane, and C is the boundary of that region. Suppose we wish to approximate $\nabla^2 \alpha$ at the point p shown in Fig. 1. As a first approximation, we can perform the line integral on the right-hand side of (1) along the path $a \to b \to c \to d \to e \to f$. Assume this is a perfect hexagon for which the length of an edge is $l_i^{(q)}$. The area of this hexagon is given by $A^{(q)} \approx 2.59808[l_i^{(q)}]^2$. Now consider the smaller hexagonal cell defined by the path $a' \to b' \to c' \to d' \to e' \to f'$. Again, the area of this smaller hexagon is given by $A^{(q+1)} \approx 2.59808[l_i^{(q+1)}]^2$. In general, we can define a sequence of ever-smaller hexagonal cells associated with grid point p as $q \to \infty$. These smaller cells are generated by bisecting the walls of the larger cells.

Define $\nabla^2 \alpha|_x \equiv f(x)$. There exists a point x_e within the hexagon of area $A^{(q)}$ such that

$$\int_{A^{(q)}} f(x) dA = A^{(q)} f(x_e). \tag{2}$$

Formally $f(x)$ can be written as a Taylor series expanded about the point p and evaluated at x_e as follows:

$$f(x_e)A^{(q)} = f(p)A^{(q)} + (x_e - p)f'(p)A^{(q)} + \frac{(x_e - p)^2}{2!} f''(p)A^{(q)} + \cdots \tag{3}$$

or with (2)

$$f(p)A^{(q)} = \int_{A^{(q)}} f(x) dA - (x_e - p)f'(p)A^{(q)} - \frac{(x_e - p)^2}{2!} f''(p)A^{(q)} - \cdots. \tag{4}$$

In the limit as $q \to \infty$, $x_e - p \to 0$. Assuming that the derivatives of f are bounded, we can write

$$\lim_{q \to \infty} \int_{A^{(q)}} \nabla^2 \alpha dA = \nabla^2 \alpha|_p \lim_{q \to \infty} A^{(q)}. \tag{5}$$

Corresponding author address: Ross Heikes, Department of Atmospheric Science, Colorado State University, Fort Collins, CO 80523.

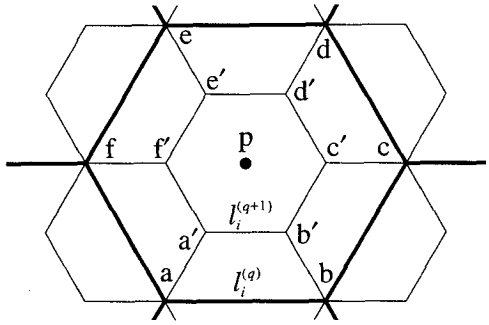

FIG. 1. Two resolutions of grid cells associated with a grid point p.

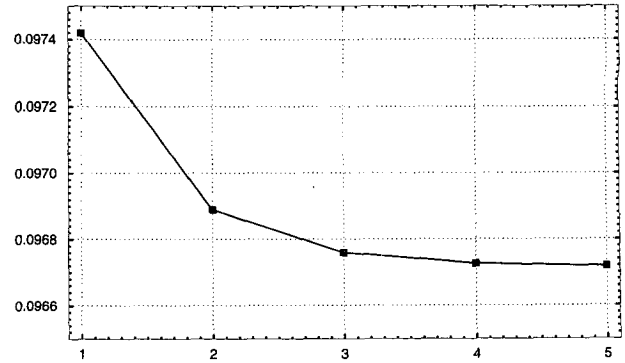

FIG. 2. Maximum ratio for the entire grid as a function of grid resolution using the simple algorithm.

Taking limits in (1) we obtain

$$\nabla^2\alpha|_p = \lim_{q\to\infty} \frac{1}{A^{(q)}} \sum_{i=1}^{6} \int_{l_i^{(q)}} \frac{\partial\alpha}{\partial n}\, dl. \tag{6}$$

Suppose we know $\partial\alpha/\partial n$ along the cell walls and for convenience define $g \equiv \partial\alpha/\partial n$. We wish to approximate the integrals on the right-hand side of (6). Consider an arbitrary hexagon side $l_i^{(q)}$ on resolution q. Without loss of generality, we can parameterize the path along edge $l_i^{(q)}$ so the origin occurs at the midpoint $m_i^{(q)} = 0$. We can write g as a Maclaurin series expanded about the midpoint of the side

$$g(x) = g[m_i^{(q)}] + xg'[m_i^{(q)}] + \frac{x^2}{2!} g''[m_i^{(q)}] + \frac{x^3}{3!} g'''[m_i^{(q)}] + \cdots. \tag{7}$$

Integrating over the length of the side we have

$$\int_{l_i^{(q)}} g(x)dl = l_i^{(q)} g[m_i^{(q)}] + \frac{[l_i^{(q)}]^3}{3(2!)} g''[m_i^{(q)}] + \cdots. \tag{8}$$

Substituting (8) into (6) we get

$$\nabla^2\alpha|_p = \lim_{q\to\infty} \frac{1}{A^{(q)}} \sum_{i=1}^{6} \left\{ l_i^{(q)} g[m_i^{(q)}] + \frac{[l_i^{(q)}]^3}{2!} g''[m_i^{(q)}] + \cdots \right\}. \tag{9}$$

Using $A^{(q)} \approx 2.59808[l_i^{(q)}]^2$ and assuming that the derivatives of g are bounded, the first terms of the series will dominate, so we can write

$$\nabla^2\alpha|_p = \lim_{q\to\infty} \frac{1}{A^{(q)}} \sum_{i=1}^{6} \{ l_i^{(q)} g[m_i^{(q)}] \}. \tag{10}$$

This means that the scheme is consistent when $\partial\alpha/\partial n$ is evaluated or, in practice, approximated at the centers of the cells walls [see Haltiner and Williams (1980)].

Now write g as a Taylor series expanded about a point $x_i^{(q)}$ along the edge wall and evaluated at $g[m_i^{(q)}]$, that is,

$$g[m_i^{(q)}] = g[x_i^{(q)}] + e_i^{(q)} g'[x_i^{(q)}] + \frac{[e_i^{(q)}]^2}{2!} g''[x_i^{(q)}] + \cdots. \tag{11}$$

Therefore $e_i^{(q)} = m_i^{(q)} - x_i^{(q)}$, where $e_i^{(q)} = r_i^{(q)} l_i^{(q)}$ and $-1 \leq r_i^{(q)} \leq 1$. That is, the distance between $x_i^{(q)}$ and $m_i^{(q)}$ is some fraction of the length of the cell wall. Multiplying both sides of (11) by $l_i^{(q)}$ gives

$$l_i^{(q)} g[m_i^{(q)}] = l_i^{(q)} g[x_i^{(q)}] + l_i^{(q)} e_i^{(q)} g'[x_i^{(q)}] + \frac{l_i^{(q)}[e_i^{(q)}]^2}{2!} g''[x_i^{(q)}] + \cdots. \tag{12}$$

Substituting into (10) and using $A^{(q)} \approx 2.59808 \times [l_i^{(q)}]^2$ and $e_i^{(q)} = r_i^{(q)} l_i^{(q)}$, we get

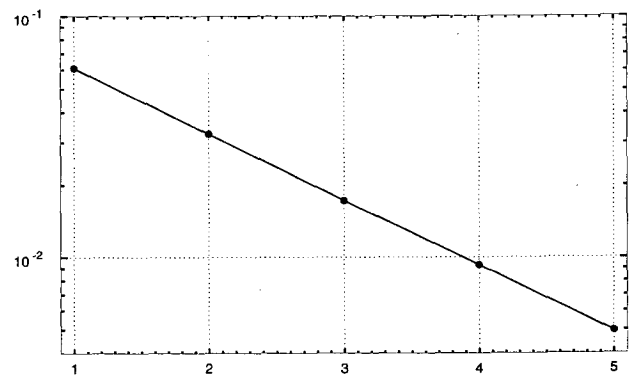

FIG. 3. Maximum ratio for the entire grid as a function of grid resolution using the improved algorithm.

TABLE 1. Properties of the improved grid as a function of recursive subdivisions of the twisted icosahedron polyhedron. See Eq. (9) and Table 1 of Part I.

q	Number of cells N_c	Number of cells along equator	Average cell area (km^2)	Ratio of smallest cell to largest cell	Average distance between cell centers (km)	Ratio of smallest distance to largest distance between cell centers
0	42	10	1.214×10^7	0.885	3755.5	0.881
1	162	20	3.149×10^6	0.868	1916.4	0.811
2	642	40	7.946×10^5	0.880	962.4	0.787
3	2562	80	1.991×10^5	0.877	481.7	0.778
4	10 242	160	4.980×10^4	0.870	240.9	0.775
5	40 962	320	1.245×10^4	0.867	120.5	0.776

$$\nabla^2\alpha|_p = \lim_{q\to\infty} \sum_{i=1}^{6} \left\{ \frac{g[x_i^{(q)}]}{l_i^{(q)}} + r_i^{(q)} g'[x_i^{(q)}] + \frac{l_i^{(q)}[r_i^{(q)}]^2}{2!} g''[x_i^{(q)}] + \cdots \right\}. \quad (13)$$

Again, the higher-order term will go to zero as $q \to \infty$, but we also require $r_i^{(q)} \to 0$ as $q \to \infty$ for consistency.

In section 4 of Part I, it was shown that the approximation to the normal derivative is applied at the midpoint of the segment connecting two cell centers. By the definition of the Voronoi cell, this point is on the cell wall shared by two grid points, but it is not necessarily the midpoint of the cell wall. Henceforth, $r_i^{(q)}$ will be defined to be the distance between the midpoint of a cell wall and the midpoint of the segment connecting two grid points divided by the length of the cell wall. We can plot $\max\{r_i^{(q)} \mid \forall \text{cells}\}$, that is, the largest $r_i^{(q)}$ for all the cell walls of grid resolution (q). The plot is shown in Fig. 2. The figure shows that using

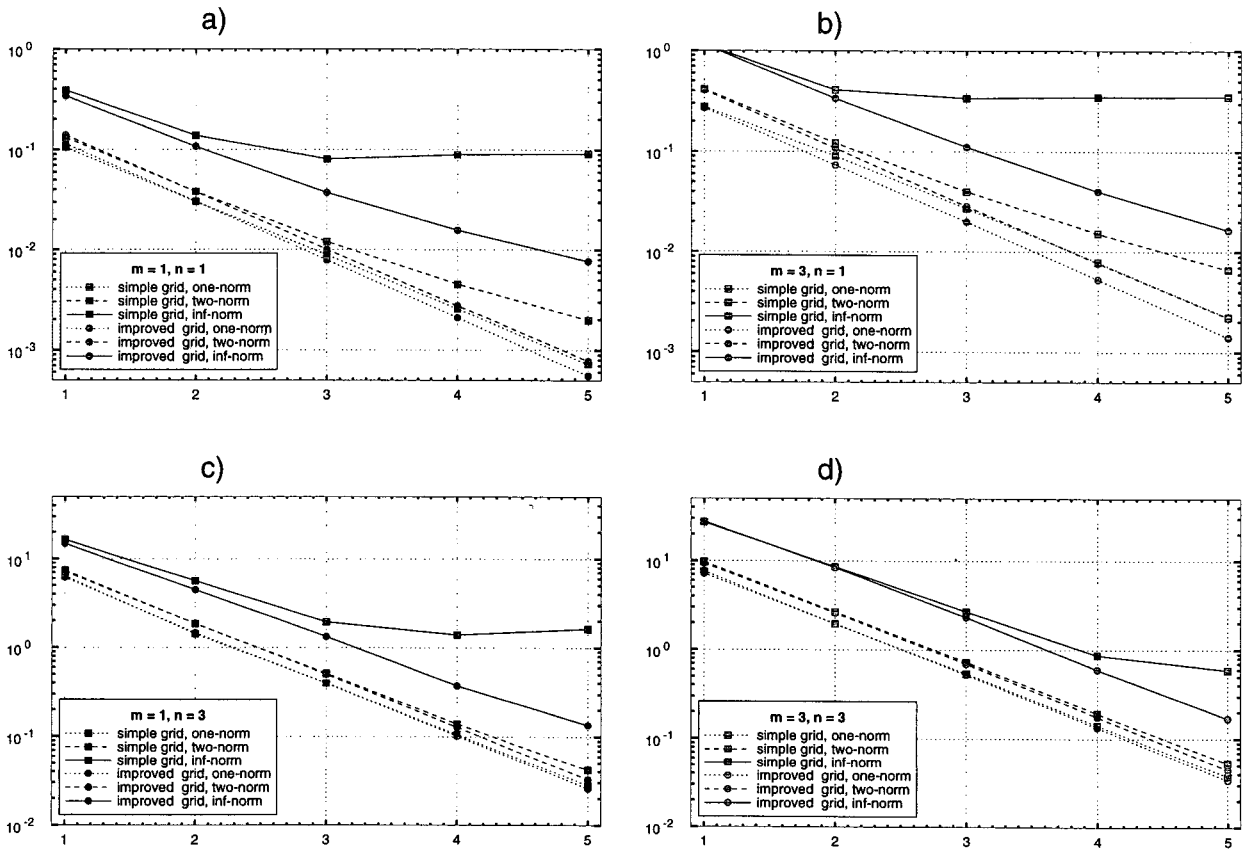

FIG. 4. Error in the finite-difference Laplace operator: (a) $m = 1$, $n = 1$; (b) $m = 3$, $n = 1$; (c) $m = 1$, $n = 3$; (d) $m = 3$, $n = 3$.

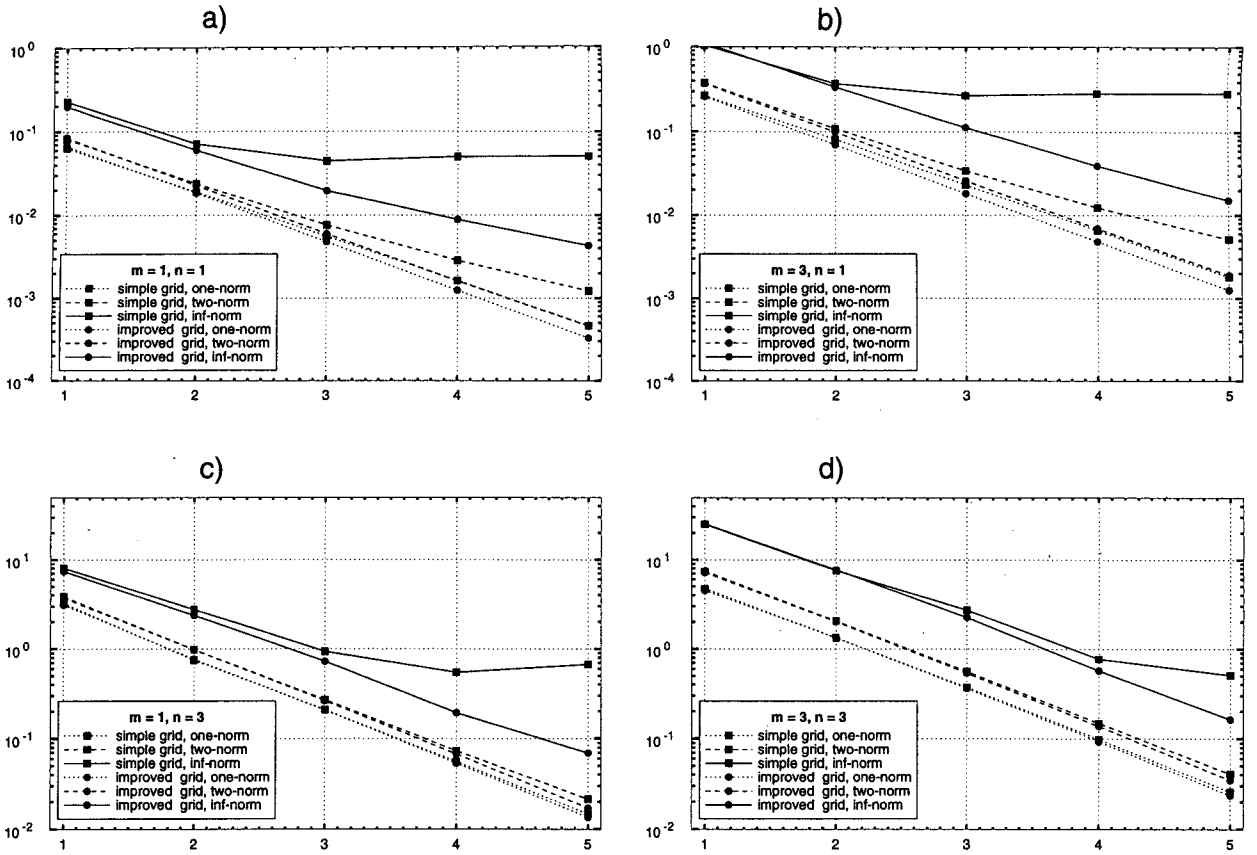

FIG. 5. Error in the finite-difference flux-divergence operator: (a) $m = 1$, $n = 1$; (b) $m = 3$, $n = 1$; (c) $m = 1$, $n = 3$; (d) $m = 3$, $n = 3$.

this simple algorithm, $r_i^{(q)}$ does not converge to zero as $q \to \infty$ for at least one cell wall on the grid, and by (13) the scheme is inconsistent for that cell. This discussion was given in the context of the Laplace operator, but clearly the normal derivative in the flux-divergence would have the same problems.

3. Design of an improved spherical geodesic grid

We have designed a simple algorithm to position the grid points that is guaranteed to reduce $\max\{r_i^{(q)} \mid \forall\text{cells}\}$ as $q \to \infty$. For a given distribution of grid points, we can calculate $\{r_i^{(q)} \mid \forall\text{cells}\}$, the set of all ratios for all cell walls. We can apply a norm to this set that will produce a single number. The choice of norm is somewhat arbitrary. Through numerical experimentation, we chose

$$R(q) = \sum_{\text{cells}} \sum_{i=1}^{s} [r_i^{(q)}]^4, \tag{14}$$

where $s = 6$ for the hexagons and $s = 5$ for the pentagons. The function $R(q)$ is a function of resolution, and more important, it is a function of the distribution of grid points. For a given resolution q, each grid point has a longitude and a latitude, so using Eq. (9) from Part I there are at most $2N_c$ independent variables to compute (14). This number can be substantially reduced by forcing the grid to be symmetric across the equator and to have a periodicity of 5 in the longitudinal direction.

Our goal is to find the distribution of grid points that minimizes (14). This can be done using quasi-Newton methods. Suppose we have a single-valued function of many variables $f(\mathbf{x})$, where $\mathbf{x} = (x_1, x_2, \cdots, x_N) \in \Re^N$ is a point in N-dimensional space. Our goal is to find $\mathbf{x}^*$ that minimizes $f(\mathbf{x})$, that is, $f(\mathbf{x}^*) = \min\{f(\mathbf{x}) | \mathbf{x} \in \Re^N\}$. This is the classical unconstrained optimization problem discussed by Fletcher (1987). There is a very efficient IMSL library call named UMINF available to perform this optimization.

Now we go back to the construction of the improved grid. The large power on $r_i^{(q)}$ in (14) quickly forces the solution away from gridpoint distributions in which a few cell walls have a very large ratio. As with the simpler algorithm, we begin with the coarsest grid and work toward increasing resolution. Define the coarsest

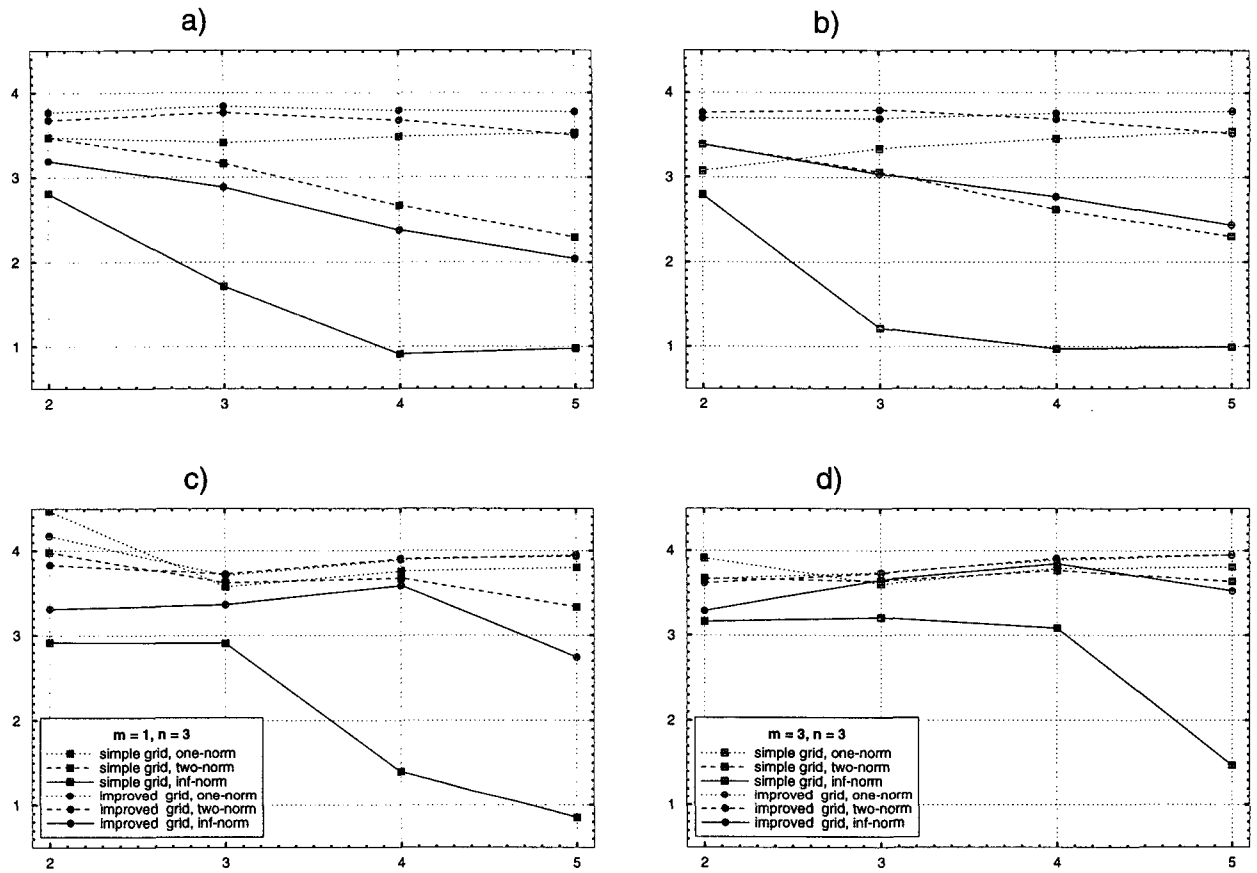

FIG. 6. Order of accuracy of the finite-difference Laplace operator: (a) $m = 1$, $n = 1$; (b) $m = 3$, $n = 1$; (c) $m = 1$, $n = 3$; (d) $m = 3$, $n = 3$.

grid, the vertices of the original twisted icosahedron, to be resolution $q = 0$. This is Fig. 1d of Part I. Similarly, define the next finer resolution, shown in Fig. 12a of the first paper, to be resolution $q = 1$, and so on. Those grid points that are members of resolution $q = 1$ but not of $q = 0$ are allowed to position themselves to minimize $R(1)$. Next, those grid points that are members of resolution $q = 2$ but not of $q = 1$ are allowed to position themselves to minimize $R(2)$. The plot of $\max\{r_i^{(q)} \mid \forall\text{cells}\}$ as a function of q is shown in Fig. 3. Note that $\max\{r_i^{(q)} \mid \forall\text{cells}\}$ appears to be converging to zero.

The point is that since the construction of the Voronoi cells does not guarantee that the point at which the normal derivative is evaluated is the midpoint of the cell wall, by Eq. (13) we must take care that the term $r_i^{(q)} \to 0$ as $q \to \infty$. This improved grid-generating algorithm has that property.

Table 1 shows some properties of the improved grid. This table should be compared with Table 1 of Part I. We see that an improved ratio of smallest cell area to largest cell area is a side effect of the improved algorithm.

4. Some observations about the errors of the finite-difference operators

To test the finite-difference operators we use the following test functions:

$$\alpha(\lambda, \theta) = \sin(\lambda), \tag{15}$$

and

$$\beta_{m,n}(\lambda, \theta) = a^2 \cos(m\lambda) \cos^4(n\theta), \tag{16}$$

where λ is longitude and θ is latitude.

The following plots show the one norm, two norm, and infinity norm of the difference between the numeric solution x^{approx} and the true solution x^{true}. The one-norm is defined by

$$\|x^{\text{approx}} - x^{\text{true}}\|_1 = \frac{1}{A_e} \sum_{\text{cells}} A_{c_i} |x_i^{\text{approx}} - x_i^{\text{true}}|, \tag{17}$$

where the summation is over all the grid points. Here A_{c_i} is the area of cell i, and $A_e = \Sigma A_{c_i}$ is the area of the planet. The two norm is defined by

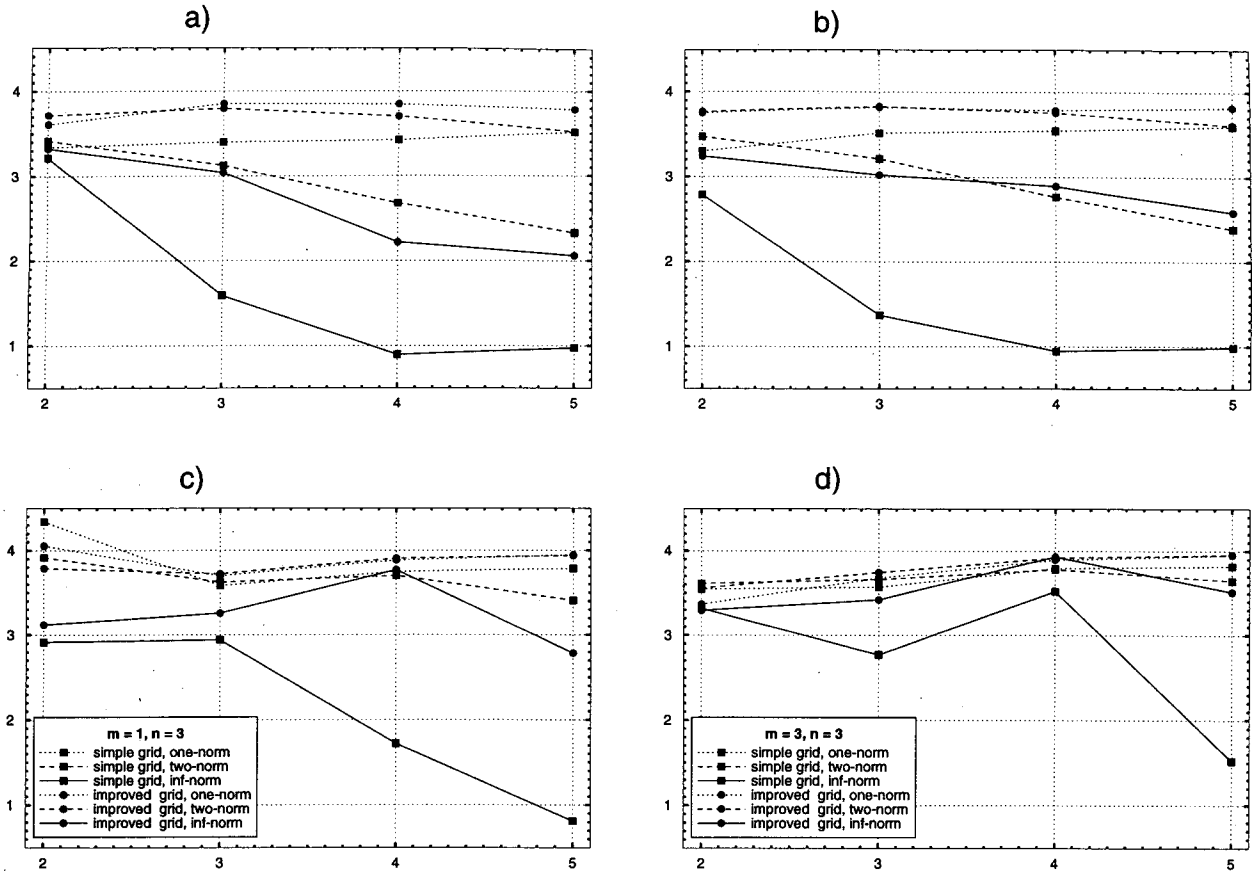

FIG. 7. Order of accuracy of the finite-difference flux-divergence operator: (a) $m = 1$, $n = 1$; (b) $m = 3$, $n = 1$; (c) $m = 1$, $n = 3$; (d) $m = 3$, $n = 3$.

$$\|x^{\text{approx}} - x^{\text{true}}\|_2 = \left[\frac{1}{A_c}\sum_{\text{cells}} A_{c_i}(x_i^{\text{approx}} - x_i^{\text{true}})^2\right]^{1/2}. \tag{18}$$

The infinity norm is defined by

$$\|x^{\text{approx}} - x^{\text{true}}\|_\infty = \max\{|x_i^{\text{approx}} - x_i^{\text{true}}| \forall \text{cells}\}. \tag{19}$$

Figures 4 and 5 show the results of applying the finite-difference Laplacian to the test function (16). In the plots, the solid line corresponds to the infinity norm, the dashed line corresponds to the two norm, and the dotted line corresponds to the one norm. The lines with the square symbol are results obtained using the simple grid and the lines with the round symbol are results obtained with the improved grid. Figure 4 shows the results from the Laplace operator when m and n in (16) are set to $m = 1, 3$ and $n = 1, 3$. The infinity-norm indicates there are certain cells on the simple grid for which the numerical solution does not converge to the analytic solution. Figure 5 shows the same thing but for the flux-divergence operator applied to (15) and (16).

5. Some observations about order of accuracy of the finite-difference operators

The irregular nature of the grid makes it difficult to analytically investigate the order of accuracy of the three operators. Suppose δ_h^2 denotes a finite-difference form of the continuous Laplace operator. If this operator is second order, then when applied to an arbitrary function α we can write

$$\nabla^2\alpha - \delta_h^2\alpha = O(h^2). \tag{20}$$

The finite-difference Laplacian is a function of both α and the grid spacing h. Suppose two different resolution grids have spacings h_1 and h_2 where $h_1 = 2h_2$. Then from (20) we get

$$\frac{\|\nabla^2\alpha - \delta_{h_1}^2\alpha\|}{\|\nabla^2\alpha - \delta_{h_2}^2\alpha\|} = \frac{O(h_1^2)}{O(h_2^2)} = \frac{O(4h_2^2)}{O(h_2^2)} = 4, \tag{21}$$

where $\|\ \|$ is some norm. In general, if the finite-difference form of the operator is kth order, following the above example we can write

$$\frac{\|\nabla^2\alpha - \delta_{h_1}^2\alpha\|}{\|\nabla^2\alpha - \delta_{h_2}^2\alpha\|} = 2^k. \tag{22}$$

The results from the Laplace operator with $n = 1$, $m = 1, 3$ and $n = 3$, $m = 1, 3$ and $n = 3$, $m = 1, 3$ are shown in Fig. 6. The results from the flux-divergence operator with $n = 1$, $m = 1, 3$ and $n = 3$, $m = 1, 3$ are shown in Fig. 7. These plots show the scheme is roughly second order. The Jacobian operator presented in Part I is also (approximately) second-order accuracy.

6. Conclusions

We have shown the Laplace operator when discretized as in Part I is consistent when the normal derivative is approximated at the center of the cell wall. Further, we have shown that for the finite-difference scheme to be consistent, it is necessary for $r_i^{(q)}$, as defined in section 2, to converge to zero as $q \to \infty$. The simple bisecting algorithm for generating finer grids from coarser ones does not have this property. We have developed an improved grid-generation algorithm that does not suffer from this problem. When implemented on these tweaked finite-difference grid, the Laplace, Jacobian, and flux-divergence operators presented in Part I have approximately second-order accuracy.

Acknowledgments. Support for this research was provided by the U.S. Department of Energy's CHAMMP Program under Grant DE-FG02-91ER61218 to Colorado State University. Computing support was provided by the National Energy Research Supercomputer Center at Lawrence Livermore National Laboratory.

REFERENCES

Fletcher, R., 1987: *Practical Methods of Optimization.* Wiley, 49 pp.

Haltiner, G. J., and R. T. Williams, 1980: *Numerical Prediction and Dynamic Meteorology.* Wiley, 120 pp.

Heikes, R., and D. A. Randall, 1995: Numerical integration of the shallow-water equations on a twisted icosahedral grid. Part I: Basic design and results of tests. *Mon. Wea. Rev.*, **123,** 1862–1880.